PAPER

Characterization and application of photocrosslinkable collagen maleate as bioink in extrusion-based 3D bioprinting†

Po-Hsun Chen,[a] I-Hsiang Chen,[a] Wei-Hsiang Kao,[a] Song-Yi Wu[a,b,c,d] and Wei-Bor Tsai [ID] *[a,b]

3D bioprinting, a significant advancement in biofabrication, is renowned for its precision in creating tissue constructs. Collagen, despite being a gold standard biomaterial, faces challenges in bioink formulations due to its unique physicochemical properties. This study introduces a novel, neutral-soluble, photocrosslinkable collagen maleate (ColME) that is ideal for 3D bioprinting. ColME was synthesized by chemically modifying bovine type I collagen with maleic anhydride, achieving a high substitution ratio that shifted the isoelectric point to enhance solubility in physiological pH environments. This modification was confirmed to preserve the collagen's triple-helix structure substantially. Bioprinting parameters for ColME were optimized, focusing on adjustments to the bioink concentration, extrusion pressure, nozzle speed, and temperature. Results demonstrated that lower temperatures and smaller nozzle sizes substantially improved the print quality of grid structures. Additionally, the application of intermittent photo-crosslinking facilitated the development of structurally robust 3D multilayered constructs, enabling the stable fabrication of complex tissues. Cell viability assays showed that encapsulated cells within the ColME matrix maintained high viability after printing. When compared to methacrylated gelatin, ColME exhibited superior mechanical strength, resistance to enzymatic digestion, and overall printability, positioning it as an outstanding bioink for the creation of durable, bioactive 3D tissues.

Introduction

Biofabrication is dedicated to the creation of three-dimensional (3D) tissue structures that closely resemble natural biological forms.[1] The advent of 3D bioprinting marks a significant advancement over traditional biofabrication techniques, celebrated for its precision in meticulously orchestrating the architecture of tissue constructs.[2,3] This technique ensures well-controlled precision and uniformity through its automated layering process, enabling the precise spatial distribution of biomaterials, living cells, and bioactive substances. Consequently, 3D bioprinting facilitates the fabrication of 3D tissues with complex, pre-defined structures and shapes, heralding a new era in biofabrication methodologies.

Bioink plays a crucial role as it aims to mimic critical aspects of the extracellular matrix (ECM), providing essential support for cell adhesion, proliferation, and differentiation to form a functional tissue. An ideal bioink is characterized by its printability, biocompatibility, suitable mechanical properties, and capacity for biomimicry with varied bioprinting techniques. Additionally, maintaining cell viability during the extrusion-printing process is a critical aspect of bioink functionality.

3D bioprinting techniques are typically classified into three main mechanisms: (1) extrusion-based, (2) jetting-based, and (3) laser-assisted bioprinting. Extrusion-based bioprinting operates through pneumatic pressure or a piston, making it particularly effective for vertical stacking.[4] However, it often involves a trade-off between structural integrity and cell viability, which can range from 40% to 98%, mainly due to the shear stress within the nozzle.[5] Jetting-based bioprinting creates patterns using micro-droplets generated by piezoelectric or thermal printheads, offering independent control over droplet size and printing speed.[6] This method achieves approximately 80% cell viability, though it is typically limited

[a]*Department of Chemical Engineering, National Taiwan University, No. 1, Sec. 4, Roosevelt Rd., Taipei 106, Taiwan. E-mail: weibortsai@ntu.edu.tw*
[b]*Program of Green Materials and Precision Devices, School of Engineering, National Taiwan University, No. 1, Sec. 4, Roosevelt Rd., Taipei 106, Taiwan*
[c]*Guangdong Victory Co., Ltd., 4F., A11, Guangdong New Light Source Industrial Park, Luocun, Shishan Town, Nanhai District, Foshan City 528226, China*
[d]*Guangxi Shenguan Collagen Biological Group Company Limited, No. 39 Xijiang 4th Rd., Wuzhou, China*
†Electronic supplementary information (ESI) available. See DOI: https://doi.org/10.1039/d4bm00826j

by the low viscosity of the bioink.[6,7] Laser-assisted bioprinting uses laser pulses to eject bioink droplets from a donor layer with high speed and precision. The high resolution of this technique is generally influenced by the viscosity and surface tension of the bioink in relation to the laser energy.[8] Additionally, this method boasts superior cell viability, typically around 90%, due to its nozzle-free system.[6,8]

Due to the simplicity of the printing mechanism, extrusion-based bioprinting was used in this study. Central to this process is the bioink's ability to quickly harden upon extrusion, thus maintaining the integrity of the designed structure.[9] With this aspect, vat polymerization-based bioprinting, which utilizes photoinitiators combined with a light source for curing bioink, offers a direct, simple, and rapid curing method.[10] The sources of photopolymerizable bioinks include synthetic or natural precursors. Synthetic precursors excel in offering precise control over molecular weight, functionality, and physiochemical characteristics at a molecular level, which facilitate accomplishment of precise control over crosslinking rates and mechanical properties. On the other hand, naturally derived biomaterials, such as alginate, gelatin, collagen, chitosan, fibrin, and hyaluronic acid, are popular as bioink constituents due to their inherent biochemical similarities with the natural ECM, biodegradability, and biological recognition.[4] However, concerns regarding the use of natural polymers include batch-to-batch variability, potential immunogenicity, narrow processing windows, and weak mechanical properties.

Within the realm of natural polymers for 3D bioprinting, gelatin and hyaluronic acid, when conjugated with methacrylate, have gained prominence for creating photoinitiated hydrogels extensively used in tissue engineering and drug delivery.[11–15] Despite gelatin's excellent biocompatibility, biodegradability, and cell affinity, methacrylated gelatin (GelMA) poses a challenge due to its narrow crosslinking window. The fluidity of GelMA is highly sensitive to temperature variations, which complicates the maintenance of bioprinted structures.[16] In contrast, collagen, a major ECM component and the most important structural protein in vertebrates, has been less frequently utilized as a precursor for 3D bioprinting. Collagen, with its robust triple-helix fibrillar structure, cannot dissolve in neutral or physiological buffers, rendering it non-printable under such conditions, though it is soluble in acidic buffers, which are incompatible with cell encapsulation.[17–20] Furthermore, the neutralization of acidic collagen solutions often leads to the formation of non-homogeneous suspensions due to fiber self-assembly, making extrusion through a nozzle challenging.[21–23] These unique physicochemical properties make collagen a challenging candidate for bioink formulations.

The challenge of rendering collagen soluble at physiological pH may be addressed through chemical modification. For instance, modifying type I collagen with succinic anhydride converts its amino groups into carboxylic groups,[24] thereby enhancing the anionic character of the collagen. This modification significantly lowers the isoelectric point of collagen, enabling its solubility in physiological pH environments.[25,26]

Similarly, collagen can be conjugated with unsaturated cyclic anhydrides, facilitating the synthesis of photocrosslinkable collagen that is compatible with physiological buffers. The conjugation with unsaturated cyclic anhydrides such as maleic anhydride, citraconic anhydride, or 2,3-dimethylmaleic anhydride endows collagen with both vinyl and carboxylic groups.[27,28] However, some previous studies have shown that these modifications often result in collagen that still requires dissolution in acidic buffers, likely due to a low degree of substitution.[27] Furthermore, these studies have primarily focused on analyzing the physicochemical properties of the modified collagen, rather than exploring its potential applications in 3D bioprinting.[27,28]

This study aimed to evaluate the suitability of neutral-soluble, maleic anhydride modified collagen for 3D bioprinting applications. Bovine type I collagen was modified with maleic anhydride to achieve a substitution ratio exceeding 90%, producing collagen maleate (ColME). A comprehensive analysis of ColME's physicochemical properties, cytocompatibility, and enzymatic digestibility was conducted. Notably, the study investigated ColME's potential for creating stable, layer-by-layer 3D structures, with a focus on the material's ability to withstand the extrusion process and maintain the integrity of the printed structures. Bioprinting parameters, including cartridge temperature, nozzle dimensions, nozzle speed, and extrusion pressures, were meticulously optimized across various ColME concentrations to ensure optimal printing conditions.

Experimental section

Synthesis of ColME and GelMA

Bovine type I collagen (COL), sourced from Victory Biotech Co., Guangdong, China, was conjugated with maleic anhydride (Thermo Scientific, USA) to synthesize ColME, following a previously established method.[28] Initially, COL was dissolved in 0.5 M acetic acid to achieve a concentration of 0.8% w/v (hereafter abbreviated as 0.8%). The pH of the solution was then adjusted to 9.0 using 1 N NaOH. A maleic anhydride solution prepared in acetone was subsequently added to the COL mixture. This mixture was incubated at 4 °C overnight with constant, gentle stirring. The resulting modified collagen underwent dialysis against a 1 mM phosphate buffer at pH 7.4, maintained at 4 °C for three days with several changes of the dialysis buffer, after which it was subjected to freeze-drying.

Gelatin methacrylate (GelMA) was synthesized using an established protocol.[29] In summary, type A gelatin (Gel; Sigma, USA) was dissolved in phosphate-buffered saline (PBS), while *N*-succinimidyl methacrylate (TCI, Japan) was prepared in dimethyl sulfoxide (J.T. Baker, USA). These two solutions were then combined to achieve final concentrations of 0.1% gelatin and 0.25% *N*-succinimidyl methacrylate. The mixture was allowed to react at room temperature for an overnight period. Subsequently, the reaction product underwent a dialysis

process against deionized water over a span of three days, followed by freeze-drying to obtain the final product.

Physiochemical characterization of ColME

The concentrations of both COL and ColME solutions were quantified using a hydroxyproline assay,[30] the details of which are provided in S1 of the ESI.† The degree of substitution (DS) of ColME was quantified by measuring the free amino groups present using the trinitrobenzenesulfonic acid (TNBS; Sigma-Aldrich, USA) colorimetric assay. Briefly, a 100 μL aliquot of a 0.1% solution of either COL or ColME was adjusted to pH 9.0 with NaOH, and subsequently diluted with a 0.1 M sodium bicarbonate buffer at pH 9.8. A 0.01% TNBS solution was then added to the sample, followed by incubation at 37 °C for one hour in a dark environment. The reaction was terminated by neutralization with 0.1 N HCl and the mixture was allowed to stand at room temperature for 30 minutes. Absorbance was measured at a wavelength of 353 nm. The concentration of amino groups in both COL and ColME samples was calculated using a standard curve derived from known concentrations of glycine. The DS was then computed using a specified equation.

$$DS = \left(1 - \frac{\text{amount of amines on ColME}}{\text{amount of amines on COL}}\right) \times 100\%$$

The characterization of modified collagen employed multiple analytical techniques. COL and ColME were analyzed using sodium dodecyl sulfate polyacrylamide gel electrophoresis (SDS-PAGE) with a 4% stacking gel and a 10% separating gel. The functional groups present in COL and ColME were identified using Fourier transform infrared (FTIR) spectroscopy, scanning the range from 4000 cm^{-1} to 500 cm^{-1} at room temperature, with a resolution of 1 cm^{-1}, employing a PerkinElmer Spectrum 100 FTIR spectrophotometer (USA). Additionally, the structural integrity of COL and ColME was assessed through circular dichroism (CD) spectroscopy using a JASCO J-815 spectrometer (Japan), with spectra recorded from 190 nm to 250 nm, a bandwidth of 1.0 nm, and a scan rate of 100 nm min^{-1}. Thermal stability assessments for COL and ColME were performed with a differential scanning calorimeter (DSC 25, TA Instruments, USA), where 5 mg samples were moistened with deionized water and sealed in aluminium pans. The DSC thermograms were obtained from 25 °C to 60 °C at a heating rate of 1 °C min^{-1}. The zeta potentials of 0.1% COL and ColME solutions at varying pH levels were measured using a Zetasizer Nano from Malvern (UK).

Rheological analysis of ColME solutions

The viscosity of the protein solutions was initially determined using a rotational viscometer (ViscoQC 100L, Anton Paar, Austria) equipped with a T-F spindle. Measurements were conducted at a constant rotation of 20 rpm. The dynamic viscosities of COL and ColME solutions at concentrations of 0.4, 0.6, and 0.8% were recorded at temperatures of 4 and 20 °C.

The rheological properties of ColME solutions at four concentrations (1.2%, 1.5%, 1.8%, 2.0%) were characterized in flow mode using a rotational rheometer (HR-2, TA

Instruments, USA) fitted with an 8 mm parallel plate geometry. A shear rate sweep from 0.001 to 1000 s^{-1} was conducted to ensure no slippage of the samples at a controlled temperature of 20 °C. Further exploration of the correlation between viscosity and shear stress was conducted through a shear rate sweep. The yield stress was determined at the point where the regression line intersected between the plateau region and the region showing a decrease in viscosity.[31,32]

Enzyme degradation assay

Enzymatic degradation of COL, ColME, Gel, and GelMA was assessed using collagenase I (C9891, Sigma-Aldrich) and matrix metalloproteinase 2 (MMP-2, SRP3118, Sigma-Aldrich). Collagenase I was prepared in a 50 mM N-[tris(hydroxymethyl) methyl]-2-aminoethanesulfonic acid (TES; T1375, Sigma-Aldrich) buffer containing 0.36 mM calcium chloride, while MMP-2 was solubilized in a 20 mM 4-(2-hydroxyethyl)piperazine-1-ethanesulfonic acid (HEPES; H3375, Sigma-Aldrich) buffer with 140 mM sodium chloride and 2 mM calcium chloride. COL, ColME, Gel, and GelMA were each prepared as a 0.25% solution in phosphate-buffered saline (PBS), to which either collagenase I or MMP-2 was added to achieve final enzyme concentrations of 20 μg mL^{-1} and 25 nM, respectively. These solutions were then incubated at 37 °C for specified durations. After incubation, the digested samples were processed for SDS-PAGE analysis. The intensity of the a$_1$ band in each sample was quantified using NIH ImageJ software and normalized against the intensity of the corresponding untreated control to assess the extent of digestion.

Fabrication and characterization of ColME and GelMA hydrogels

ColME and GelMA hydrogels were synthesized via photo-initiation using lithium phenyl-2,4,6-trimethylbenzoyl-phosphinate (LAP; 900889, Sigma-Aldrich, USA) as the photo-initiator. The ColME solution was prepared at a concentration of 0.8%, and the GelMA solution at 3.2%, with LAP added to reach a final concentration of 0.6 mg mL^{-1} in both solutions. These mixtures were then subjected to UV irradiation at 365 nm with an intensity of 100 mW cm^{-2} for one minute to form the hydrogels.

The mechanical properties of the hydrogels were evaluated using axial compression tests conducted with a rheometer (HR 10, TA Instruments, USA). Both ColME and GelMA hydrogels were shaped in cylindrical molds with a 20 mm diameter. During testing, each hydrogel was compressed at a rate of 0.6 mm sec^{-1} until fracture occurred. The Young's modulus was calculated from the initial linear portion of the stress–strain curve, considering deformations less than 40% strain.

Hydrogel hydration levels were quantified by immersing freeze-dried hydrogels in 1 mL of phosphate-buffered saline (PBS) at 37 °C. The wet weight of the hydrogels was recorded at specified intervals, and the water content was determined based on the ratio of the wet to dry weight.

The enzymatic resistance of ColME and GelMA hydrogels to degradation was assessed in the presence of collagenase

I. Hydrogel specimens were incubated in a 10 μg mL^{-1} collagenase I solution at 37 °C. At designated time points, the residual mass of the hydrogels was collected, freeze-dried, and weighed. The degradation rate was calculated as the percentage of the final dry weight relative to the initial dry weight.

Bioprinting of ColME

Bioprinting was conducted using a pneumatic-based extrusion bioprinter (Allevi 1 and 3D Systems, Allevi, USA). A three-dimensional square structure measuring 16.0 mm in length was designed using SolidWorks software provided by 3D Systems. The gap distance between the nozzle and the printer bed was precisely set to 0.1 mm.

ColME was dissolved in a serum-free culture medium consisting of Dulbecco's modified Eagle's medium (DMEM; Gibco, USA), 1.5% antibiotic–antimycotic solution (Hyclone, USA), 110 mg L^{-1} sodium pyruvate (Sigma, USA), and 0.6 mg mL^{-1} LAP. The printability of the ColME hydrogels was evaluated using a grid infill pattern with a length of 16.0 mm and a spacing of 2.0 mm, as detailed in S2 of the ESI.† This preliminary analysis assessed various parameters including ColME concentrations, extrusion pressures, cartridge temperatures, nozzle sizes, and nozzle speeds. Nozzle sizes of 20-gauge (20G) and 25-gauge (25G), with inner diameters of 0.603 mm and 0.260 mm respectively, were used for printing. After printing, the constructs underwent UV crosslinking at an intensity of 10 mW cm^{-2} for 15 seconds. The volumetric flow rates of the ColME solution during printing were determined from the mass flow rates of samples collected over a period of 60 seconds.

Characterization of printed grid structure

Microscopic images of the printed structures were captured using an inverted microscope (IX71, Olympus, Japan) and subsequently analyzed with NIH ImageJ software. The widths of the deposited filaments were calculated using the equation provided below:

$$\text{Filament width (mm)} = \frac{\text{area of the filament}}{\text{average length of the filament}}$$

The area enclosed by filaments was quantified by measuring the spaced areas using NIH ImageJ software. Shape fidelity was assessed by observing phenomena such as the fusion of adjacent filaments, the collapse of filaments, and their subsequent impact on the circularity of the spaced areas.[33] Printability (Pr) was then evaluated based on the circularity of these spaced areas, providing a quantitative measure of the bioprinted structure's accuracy and integrity:[34]

$$\text{Printability (Pr)} = \frac{L^2}{16A}$$

where L is the perimeter, and A is the spaced area.

Fabrication of multilayered 3D bioprinted structure

Two types of multilayered 3D structures, grid and tube, were printed using a 25G nozzle. The bioprinting was conducted at a nozzle speed of 1.0 mm sec^{-1}, with the cartridge temperature set at 4 °C. The grid structure consisted of twenty layers, each measuring 18.0 mm in length with a 2.0 mm spacing between lines. UV light at 10 mW cm^{-2} was applied for 15 seconds to photo-crosslink the structure after every four layers were printed.

The tubular structure was fabricated with an inner diameter of 2.5 mm, an outer diameter of 6.0 mm, and a height of 5.0 mm. Each layer of this tube was constructed using three concentric infill patterns, printed at a faster nozzle speed of 3.0 mm sec^{-1} to accommodate the cylindrical geometry. During printing, this structure underwent two rounds of photo-crosslinking under UV light at 10 mW cm^{-2} for 15 seconds each, ensuring stability and integrity of the tubular form.

Assessment of cell viability in 3D printed ColME hydrogels

A cell-laden bioink containing 1×10^6 cells per mL of L929 mouse fibroblasts (Food Industry Research and Development Institute, Taiwan) in a ColME solution was prepared. The bioinks were extruded through a 20G or 25G nozzle under various pressures and then subjected to UV irradiation at 10 mW cm^{-2} for 30 seconds. Following irradiation, the cell-laden ColME hydrogel was cultured in Dulbecco's modified Eagle's medium (DMEM) supplemented with 1% antibiotic–antimycotic solution, 110 mg L^{-1} sodium pyruvate, and 10% fetal bovine serum (Peak Serum, USA). After two days of cultivation, cell viability was assessed using the LIVE/DEAD cell viability assay (Invitrogen, USA). Fluorescent images capturing both live (green) and dead (red) cells were obtained with an inverted fluorescence microscope (IX 71, Olympus, Japan). Quantitative analysis of cell viability was performed by counting live and dead cells using NIH ImageJ software. Cell viability was calculated as the ratio of live cells to the total number of cells (live plus dead).

Statistical analysis

Statistical analyses between all groups were performed by Prism 9 (GraphPad, USA) using the one-way or two-way ANOVA followed by Tukey's multiple comparison test. A p-value of 0.05 or less was considered statistically significant. All the values were presented as mean ± standard deviation.

Results and discussion

Physiochemical characterization of ColME

In the process of collagen modification, cyclic maleic anhydride was conjugated to the amino side chains of collagen via amide linkage formation. The degree of substitution (DS), which reflects the proportion of modified amino residues, was determined to be 98.46%, indicating an extensive substitution of amino groups with anionic carboxylic groups. Fourier-transform infrared (FTIR) analysis of collagen maleate (ColME) showed negligible differences compared to COL, as illustrated in S3 of the ESI.† Characteristic amide bands for ColME, including amide A, amide I, amide II, and amide III,[20] retained

their positions post-modification, mirroring those in the COL spectrum. This lack of spectral shift can likely be attributed to the abundant pre-existing amide bonds in COL, making the spectral contributions of additional amide linkages indistinguishable. Moreover, the absorbance ratio of the Amide III band to that at 1450 cm^{-1} (A_{III}/A_{1450}) was calculated to assess the integrity of the collagen's triple helix structure.[20,35] The A_{III}/A_{1450} ratios for COL and ColME were 0.944 and 0.978, respectively, indicating a high degree of retention of the triple helix configuration after modification.

Two a$_1$ chains and one a$_2$ chain, components of the collagen triple helix structure comprising were resolved using SDS-PAGE analysis, as depicted in Fig. 1A. The modification with maleic anhydride resulted in a discernible retardation in the electrophoretic mobility of the a$_1$ and a$_2$ chains. This retardation indicates an increase in molecular weight due to the addition of maleic anhydride groups. Notably, the absence of new bands below the a$_1$ and a$_2$ chains suggests that the modification process did not lead to significant fragmentation of the collagen.

CD analysis is a commonly employed technique to probe the secondary structure of proteins.[36] In the CD spectra presented in Fig. 1B, both COL and ColME displayed a characteristic positive band at 220 nm and a negative band at 197 nm, confirming the presence of a triple helix structure.[36] Notably, the ColME spectrum did not show ellipticity readings above 210 nm, typically indicative of disordered or denatured proteins,[36] suggesting that ColME maintained an orderly structure. Additionally, the ratio of the dichroic intensity between the positive and negative peaks, a measure of triple helix integrity,[20] yielded values of 0.129 for COL and 0.127 for ColME. These ratios further substantiate that the triple helix configuration of collagen is predominantly preserved following modification with maleic anhydride.

The isoelectric point (pI) of a protein, defined as the pH at which its net charge is zero, typically correlates with minimal solubility, thereby promoting protein aggregation and precipitation. For COL, the zeta potential was +17 mV at pH 5, which shifted to approximately −4 mV at pH 8, as illustrated in Fig. 1C. The pI of COL was estimated to be around pH 7.7, indicating compromised solubility near the physiological pH range. Upon conjugation with maleic anhydride, the amino groups in COL were replaced by carboxylic groups, making ColME more negatively charged. Specifically, the zeta potential of ColME was about +10 mV at pH 3.0, shifting to zero near pH 3.5. This shift in the pI of ColME towards a more acidic pH indicates that ColME is prone to precipitation at lower pH levels but remains soluble under neutral pH conditions.

DSC was utilized to assess the thermal stability of COL and ColME. The DSC analysis revealed that the thermal transition midpoint (T_m) of ColME occurred at 39.06 °C, which is lower than the T_m of COL, recorded at 43.82 °C, as illustrated in Fig. 1D. Additionally, the enthalpy of unfolding (ΔH) for ColME was determined to be 2.96 J g^{-1}, compared to a higher ΔH of 5.61 J g^{-1} for COL. These findings indicate a reduction in the thermal stability of collagen following its modification. Although the primary structure of the triple helix in ColME was largely preserved, a noticeable decrease in thermal stability was observed.

Rheological properties of native collagen, gelatin and the methacrylated derivatives

The rheological properties of bioinks are crucial for successful 3D bioprinting. It is well-established that bioinks with a viscosity ranging from 30 mPa·s to over 6 × 10^7 mPa·s are suitable for extrusion-based bioprinting techniques[4] Materials with higher viscosities provide essential structural integrity to bioprinted constructs, whereas materials with lower viscosities are advantageous for preserving cell viability and functionality. Initially, we assessed the viscosity of ColME to determine its suitability for bioprinting applications.

At 4 °C, COL displayed viscosities of 2.350, 5.585, and 10.112 Pa·s at concentrations of 0.4%, 0.6%, and 0.8%, respectively (Fig. 2A). Increasing the temperature to 20 °C had a minimal effect on its viscosity. In contrast, at the same concentrations and temperature, ColME exhibited lower viscosities than COL, with values of 0.391, 1.359, and 4.905 Pa·s, respectively. The reduced viscosity of ColME can be attributed to an increase in anionic charges, which diminish intramolecular interactions. Compared to GelMA at 37 °C, the viscosities of ColME and GelMA were similar, recording 0.199 and 0.225 Pa·s, respectively (Fig. 2B). GelMA showed a significant increase in viscosity as the temperature decreased, reaching 2.400 and 9.327 Pa·s at 25 °C and 20 °C, respectively. Below 10 °C, GelMA transitioned to a solid state that could not flow. In contrast, ColME's viscosity gradually increased as the temperature decreased, reaching 3.385 Pa·s at 4 °C, and remained within a relatively narrow range from 4 °C to 37 °C. This behavior highlights ColME's potential utility in applications that require precise viscosity control across a broad temperature spectrum.
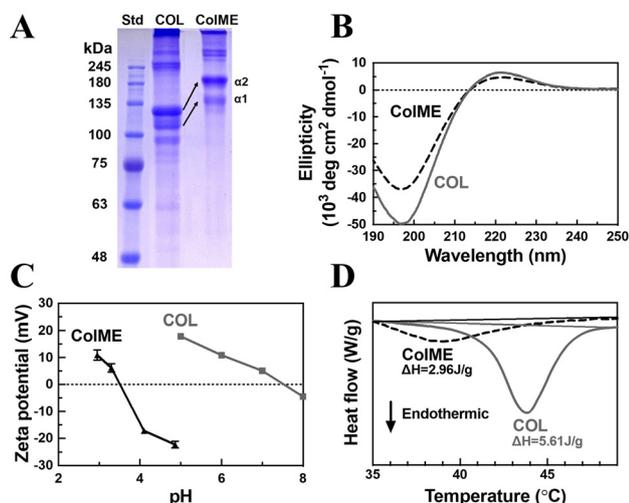

Fig. 1 Characterization of COL and ColME. (A) SDS-PAGE analysis using 4% stacking gel and 10% separating gel. Std, standard markers; (B) CD spectra from 190 to 250 nm with 1.0 nm bandwidth and 100 nm min^{-1} scanning speed; (C) zeta potential analysis at different pHs; (D) DSC analysis from 35 °C to 50 °C. ΔH indicates the enthalpy of unfolding.
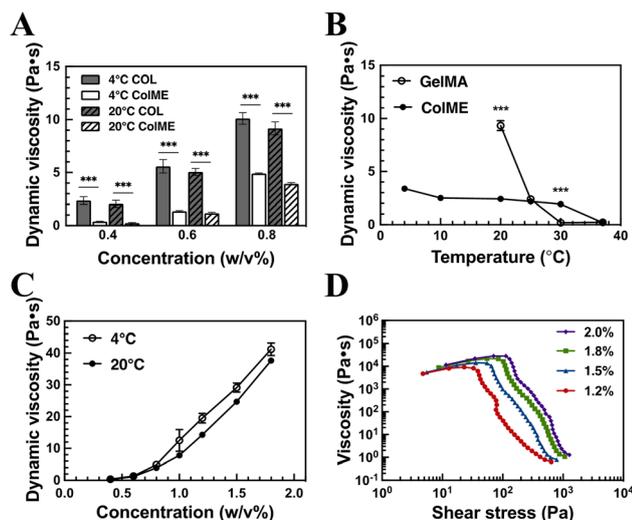
Fig. 2 Dynamic viscosity determination of COL, ColME, and GelMA. (A) Viscosities of COL and ColME at concentrations of 0.4%, 0.6%, and 0.8% measured at temperatures of 4 °C and 20 °C. (B) Viscosity profiles of ColME (0.7%) and GelMA (3.0%) across a temperature range from 4 °C to 37 °C. (C) Viscosities of ColME at concentrations ranging from 0.4% to 2.0%, measured from 4 °C to 20 °C. (D) Viscosity responses of ColME at concentrations from 1.2% to 2.0% under varying shear stresses at 20 °C.

We further explored more rheological assessments of ColME solutions at concentrations ranging from 0.4% to 2.0% (Fig. 2C). Specifically, at 4 °C, the viscosity readings escalated from 0.391 to 41.235 Pa·s for concentrations of 0.4 and 1.8 w/v%, respectively, while at 20 °C, the viscosity rose from 0.246 to 37.640 Pa·s.

We next examined the relationship between viscosities and shear stresses for ColME, which is crucial for understanding its extrusion through nozzles under varying pressures. At low shear stresses below 23.9 Pa, the viscosity of 1.2% ColME gradually increased from 4767.3 to 9170.4 Pa·s, before experiencing a sharp decrease to 0.6 Pa·s at a shear stress of 637.4 Pa (Fig. 2D). This shear-thinning behavior was consistent across higher ColME concentrations of 1.5%, 1.8%, and 2.0%. Such shear-thinning is particularly advantageous for bioprinting, as it allows the ColME solution to 'solidify' after being extruded through a nozzle by applied pressure and deposited onto a bioprinting platform. The transition point, marked by the yield stress, was determined at the intersection of the regression lines from the plateau and the decreasing viscosity regions. Yield stress values were calculated to be 25.7, 53.9, 78.4, and 105.9 Pa for ColME concentrations of 1.2%, 1.5%, 1.8%, and 2.0%, respectively. Correspondingly, the minimum extrusion pressures required for these concentrations increased to 23.2, 25.5, 26.5, and 29.2 psi at 20 °C, as shown in S4 of the ESI.†

Enzymatic degradation of modified and unmodified collagen and gelatin

The susceptibility of collagen to digestion by specific proteases, particularly the matrix metalloproteinase (MMP) family, is a critical factor given their significant role in modu-

lating cellular activities within the ECM.[37] Notably, the proline-X-glycine motif is recognized as a conventional MMP-sensitive site.[38] *In vivo*, collagens are typically first cleaved by collagenases and then undergo rapid denaturation at body temperature, facilitating further degradation by gelatinases and a range of non-specific tissue proteases.

In this study, the degradation of COL, ColME, GEL, and GelMA was examined in the presence of collagenases, including collagenase I (MMP1), which targets type I, II, III, VII, and X collagens,[39] and MMP-2, also known as gelatinase A. The digestion products were analyzed using SDS-PAGE, as depicted in S5 of the ESI.† Observations revealed that COL underwent modest digestion by both collagenase I and MMP-2, whereas ColME exhibited more pronounced digestion, evidenced by the diminished intensity of the a_1 and a_2 bands and the emergence of lower molecular weight protein fragments, suggesting enhanced accessibility of ColME to enzymatic action. Correlating with the DSC findings presented in Fig. 1D, ColME's structure appeared more disrupted, making it more susceptible to enzymatic breakdown. In contrast, gelatin was enzymatically degraded considerably faster than both COL and ColME. Notably, GelMA was completely digested within just 4 hours of MMP-2 treatment.

The extent of enzymatic digestion was quantified by evaluating the intensities of the a_1 bands, which were then normalized against those of the undigested samples. After 60 minutes of exposure to collagenase I, approximately 50% of COL remained undigested, while the majority of ColME had already been broken down within 50 minutes (Fig. 3A). Both GEL and GelMA underwent complete degradation in just 10 minutes. MMP-2 managed to cleave around 40% of COL or ColME over a span of 12 hours, in stark contrast to Gel and GelMA, which were entirely digested within 12 and 4 hours, respectively, as shown in Fig. 3B. These findings highlight that both collagen and gelatin are more susceptible to enzymatic digestion following modification. However, ColME's resistance to enzymatic degradation was markedly higher than that of GEL and GelMA.

Formation and characterization of ColME and GelMA hydrogels

We initially determined the minimum concentrations of ColME and GelMA required to form a hydrogel with sufficient
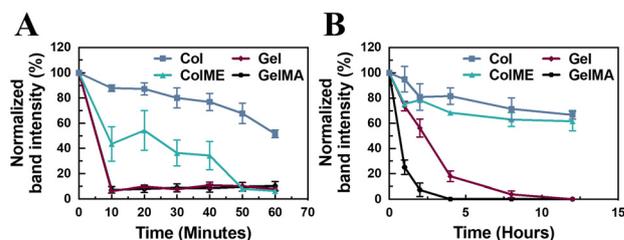

Fig. 3 Quantification of intensity of a_1 bands (from SDS-PAGE images in S5 of the ESI†) after digestion of (A) collagenase I and (B) MMP-2. Number of samples = 4.

strength. Hydrogels containing 0.8% ColME or 3.2% GelMA, each supplemented with LAP, were formed immediately upon exposure to UV light and exhibited sufficient structural integrity to withstand manipulation with a spatula, as demonstrated in S6 of the ESI.† The mechanical characteristics of these hydrogels were then evaluated by subjecting them to compression tests until fracture occurred (Fig. 4A). The ColME hydrogel displayed a Young's modulus of 41.2 kPa, which was lower than the 70.6 kPa observed for the GelMA hydrogel. This lower modulus for ColME is likely attributable to its lower concentration and testing at room temperature. In contrast, the stress required to rupture the ColME hydrogel was 94.9 kPa, substantially higher than the 20.5 kPa required for the GelMA hydrogel. Additionally, both the storage modulus (G') and the loss modulus (G'') of the ColME hydrogel were significantly higher than those of the GelMA hydrogel (Fig. 4B). These results suggest that the inherent triple-helix fibrous structure of collagen in the ColME hydrogel may contribute to its enhanced mechanical strength, compared to the GelMA hydrogel, which possesses a random coil structure.

The water uptake of ColME and GelMA hydrogels was evaluated by immersing them in PBS over time. Both types of hydrogels reached a saturation point after a 2-hour immersion period (Fig. 4C). The ColME hydrogel exhibited superior absorption capabilities, assimilating approximately 20 times its dry weight, which is higher than the 11-fold absorption observed with the GelMA hydrogel.

The enzymatic degradability of ColME and GelMA hydrogels was assessed using collagenase I. After 2 hours of digestion, the GelMA hydrogel was reduced to 8% of its original weight, whereas the ColME hydrogel retained about 25% of its mass (Fig. 4D). This indicates that ColME hydrogels have better resistance to enzymatic degradation compared to GelMA hydrogels. The enhanced durability to enzymatic degradation makes ColME hydrogels more suitable for tissue engineering applications.

Collagen is known to support cell attachment and proliferation due to its cell adhesion motifs and ECM-mimicking structures.[40] The suitability of the ColME hydrogel for cell culture was subsequently evaluated (S7 of ESI†). Initially, L929 cells demonstrated good attachment to the ColME hydrogel, and all were viable. Furthermore, the encapsulation of L929 cells in both ColME and GelMA hydrogels did not significantly compromise cell viability, as evidenced by live/dead staining images. Although the viability of L929 cells in the ColME hydrogel was comparable to that in the GelMA hydrogel, a greater number of spreading cells were observed in the ColME hydrogel, as compared to those in the GelMA hydrogel. Additionally, both the ColME and GelMA hydrogels facilitated cell proliferation. These findings demonstrate the cytocompatibility of ColME, highlighting its potential applicability as a bioink.

Optimization of bioprinting parameters for enhanced printability and structural integrity of ColME hydrogels

We next studied the impacts of three parameters—ColME concentration, extrusion pressure, and nozzle speed—on the printing quality of a grid structure. Initially, we determined the minimal extrusion pressure required to fluidize the ColME solutions through a 25G nozzle at 4 °C. The minimum extrusion pressure needed increased with the concentration of ColME: 27.0, 27.7, 29.2, and 32.2 psi for concentrations of 1.2%, 1.5%, 1.8%, and 2.0% respectively, with corresponding flow rates of 2.40, 4.59, 0.61, and 0.92 µL min^{-1} (Table 1). However, these minimal pressures proved inadequate for producing continuous filaments, necessitating increments of 1.0, 2.0, and 3.0 psi to enhance flow rate and facilitate effective bioprinting. At these adjusted pressures, the flow rates for the 1.2% ColME solution increased significantly to 3.11, 16.75, and 72.26 µL min^{-1} at 28, 29, and 30 psi, respectively. In con-
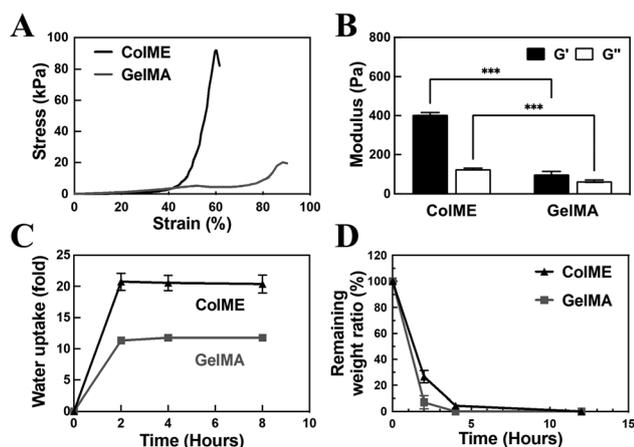

Fig. 4 Comparative analysis of ColME (0.8%) and GelMA (3.2%) hydrogels: (A) stress–strain curves from compression tests; (B) storage modulus (G') and loss modulus (G'') for both hydrogels; (C) water uptake measurements; (D) degradation profiles following exposure to Collagenase I. Number of samples = 4.

Table 1 The volumetric flow rates (V, µL min^{-1}) were measured at various ColME concentrations with different extrusion pressures (P_{ex}) at 4 °C. Number of samples = 5

ColME (w/v%)	P_{ex} (psi)	V (µL min^{-1})
1.2%	27.0	2.40 ± 0.48
	28.0	3.11 ± 0.24
	29.0	16.75 ± 6.43
	30.0	72.26 ± 1.86
1.5%	27.7	4.59 ± 0.58
	28.7	7.02 ± 2.35
	29.7	10.15 ± 0.60
	30.7	13.27 ± 2.67
1.8%	29.2	0.61 ± 0.10
	30.2	0.63 ± 0.20
	31.2	0.72 ± 0.17
	32.2	0.95 ± 0.12
2.0%	32.2	0.92 ± 0.11
	33.2	1.48 ± 0.30
	34.2	2.12 ± 0.30
	35.2	3.57 ± 0.14

trast, the increases in flow rate for the 1.5%, 1.8%, and 2.0% ColME solutions with a 3.0 psi increase were only 1.5 to 4 folds, indicating less sensitivity to pressure increments.

Extrusion of ColME solution does not guarantee achievement of the desired grid pattern. As depicted in Fig. 5, printing failures can manifest as discontinuous filaments or closure of spaced areas. This closure typically occurs due to the fusion of adjacent filaments at lower ColME concentrations (1.2% and 1.5%) under conditions of slow nozzle speeds and high extrusion pressures, as detailed in blue in Fig. 5. Specifically, closure was observed at a nozzle speed of 1.0 mm sec^{-1} for a 1.2% solution at extrusion pressures of 28.0, 29.0, and 30.0 psi, and at 3.0 mm sec^{-1} at 30.0 psi. For the 1.5% solution, closure occurred at extrusion pressures of 29.7 and 30.7 psi at a nozzle speed of 1.0 mm sec^{-1}. No closure was noted at higher concentrations of 1.8% and 2.0%. Conversely, high nozzle speeds, such as 5 mm sec^{-1} or more, may lead to filament discontinuity, as indicated in red in Fig. 5. However, higher extrusion pressures that enhance flow rates can counteract the effect of high nozzle speeds, thus ensuring continuous filaments. For example, extruding 2.0% ColME at 35.2 psi maintained continuous filaments across all tested nozzle speeds. Notably, the printable range of 1.8% ColME was narrower compared to other concentrations, *i.e.*, with nozzle speeds above 7 mm sec^{-1} failing to produce continuous filaments. The inferior printability of the 1.8% ColME may be due to its lower volumetric flow rate, although the specific cause of this reduced flow rate remains unclear.

Next, we employed the parameter 'printability' (Pr),[41] which evaluates the spatial geometry of printed structures through circularity measurements, serving as a metric for shape fidelity. It is generally accepted that a Pr value close to unity signifies optimal printing conditions.[34] Consequently, a Pr value below 1 indicates suboptimal printability, typically resulting from insufficient viscosity or inadequate gelation of the bioink, while a Pr value above 1 suggests excessive gelation or viscosity during the bioprinting process. Microscopic images of the printed grids are presented in S8 of the ESI.† Our results indicated that all measured Pr values were below 1 across all ColME concentrations, nozzle speeds, and extrusion pressures (Fig. 5), implying that the ColME solutions are not too viscous for bioprinting. The lowest Pr observed was approximately 0.85 for 1.2% ColME concentration. Conversely, Pr values for concentrations higher than 1.5% generally exceeded 0.9. The optimal printability, approximately 0.95, was achieved with 2.0% ColME extruded at pressures of 34.2 or 35.2 psi and a nozzle speed exceeding 7 mm sec^{-1}. Notably, increasing the nozzle speed proved to be an effective strategy for enhancing printability.

We further investigated the dimensions of filaments under various bioprinting conditions, as illustrated in Fig. 6A–D. A consistent trend was observed across all ColME concentrations, where filament widths decreased with increasing nozzle speeds. Conversely, an increase in extrusion pressure resulted in wider filaments. Filaments printed from 1.2% ColME were generally wider than those from other concentrations, achieving a maximum width of 1.19 mm at a nozzle speed of 5 mm sec^{-1} (Fig. 6A). The filament widths for 1.5% ColME ranged from 0.32 to 0.90 mm (Fig. 6B), which was a broader range than observed with 1.2% ColME. The printing

ColME (w/v%)	P$_{ex}$ (psi)	Nozzle speed (mm/sec)						
		1.0	3.0	5.0	7.0	9.0	11.0	13.0
1.2%	28.0		0.840	0.886				
	29.0		0.835	0.870	0.850			
	30.0			0.835	0.838	0.858		
1.5%	28.7	0.900	0.919					
	29.7		0.888	0.933	0.941	0.939		
	30.7		0.867	0.881	0.906	0.911	0.944	
1.8%	30.2	0.921	0.972					
	31.2	0.906	0.941	0.948				
	32.2	0.896	0.924	0.948				
2.0%	33.2	0.950	0.938	0.912				
	34.2	0.910	0.932	0.925	0.957	0.955		
	35.2	0.904	0.903	0.904	0.917	0.940	0.950	0.947

Closure of spaced area
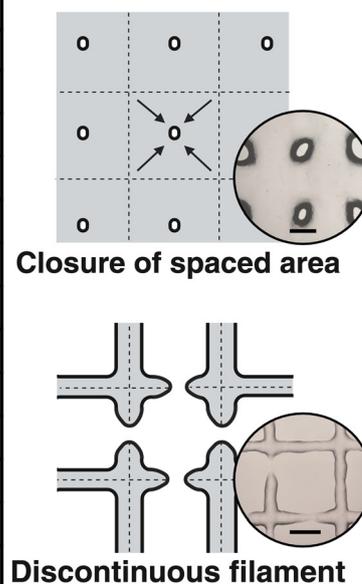
Discontinuous filament

Fig. 5 The printability (Pr, in green blocks) of various ColME concentrations is presented along with corresponding extrusion pressures (P$_{ex}$) and nozzle speeds at 4 °C. Blue blocks indicate the closure of spaced areas, while red blocks signify the presence of discontinuous filaments. A schematic diagram is included to illustrate conditions deemed 'not printable', which involve both the closure of spaced areas and the occurrence of discontinuous filaments. Scale bar = 1.0 mm. All standard deviations of printability (Pr) values are within 3.6% of the mean. Number of samples = 8.
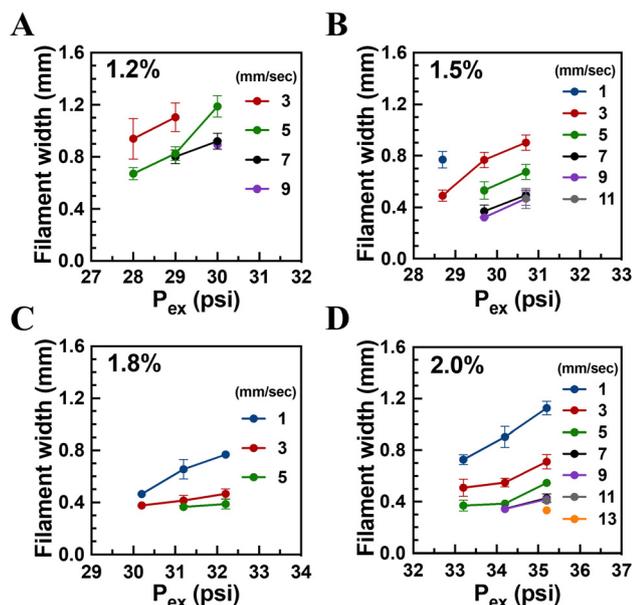
Fig. 6 Filament width was measured by varying extrusion pressures (P_{ex}) and nozzle speeds for (A) 1.2, (B) 1.5%, (C)1.8%, and (D) 2.0% ColME with a 25G nozzle at 4 °C. Number of samples = 8.

conditions for 1.8% ColME limited filament widths to a range between 0.37 and 0.77 mm (Fig. 6C). Notably, 2.0% ColME exhibited the widest range of filament widths, from 0.33 to 1.13 mm (Fig. 6D), especially at the highest extrusion pressure of 35.2 psi, where filament width could be precisely controlled by adjusting nozzle speeds. Our results indicate that filament widths can be more effectively controlled using higher concentrations of ColME combined with increased extrusion pressures.

Influence of cartridge temperature and nozzle size on the printability of ColME hydrogels

We next evaluated the impact of two additional parameters—cartridge temperature (4 °C and 20 °C) and nozzle sizes (20G and 25G)—on the printing quality of grid structures. As shown in Fig. 7A, the filaments were transparent and homogeneous, indicating no apparent fiber generation during extrusion. Notably, closure of the grid pattern was observed with 1.2% and 1.5% ColME when extruded through a 20G nozzle. Conversely, 1.8% and 2.0% ColME were successfully printed into acceptable grid structures through a 20G nozzle, though these structures were not as fine as those produced with a 25G nozzle. Filaments printed through a 20G nozzle were significantly wider than those from a 25G nozzle (Fig. 7B). Specifically, filament widths from 1.8% ColME printed through a 20G nozzle were almost twice those produced through a 25G nozzle. Accordingly, the spaced areas were smaller when using a 20G nozzle compared to a 25G nozzle (Fig. 7C), with the spaced areas of grids from 1.8% ColME through a 20G nozzle being less than half of those through a 25G nozzle.
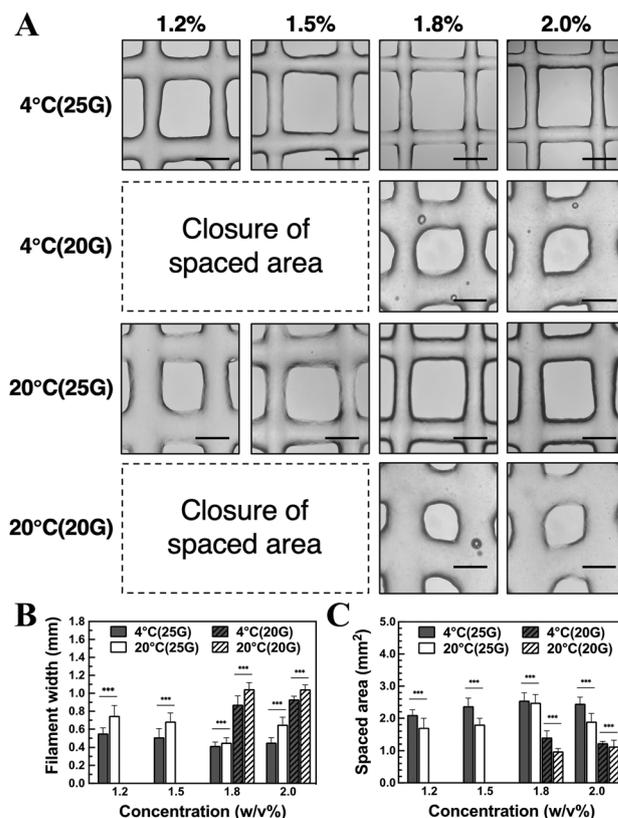

Fig. 7 (A) Optical microscopic images displaying filaments and spaced areas under varying bioprinting parameters for ColME. Scale bars = 1.0 mm. Quantitative analyses of (B) filament widths and (C) spaced areas are shown, demonstrating variations across different nozzle sizes, ColME concentrations, and temperatures. Nozzle sizes of 20G and 25G indicate 0.603 and 0.260 mm of inner diameter, respectively. Number of samples = 24.

Lower temperatures generally facilitated the production of finer grid structures. Grid structures printed from 4 °C ColME had thinner filaments and larger spaced areas compared to those from 20 °C ColME (Fig. 7B and C), suggesting that ColME filament expansion increases with temperature. This behavior is likely due to an increase in the viscosity of the ColME solution at lower temperatures (Fig. 2B). However, ColME is less temperature sensitive compared to GelMA, which is solidified at 4 °C and not suitable for printing.

Optimizing multilayered 3D structures of ColME bioprinting

We next assessed the feasibility of vertically stacking ColME filaments. Without post-bioprinting photo-crosslinking, the 3D multilayered structures often exhibited deformation, characterized by widening filaments and shrinking spaced areas in the lower layers. This resulted in a gradient decrease in printing quality from the upper to the lower layers. To address this issue, we developed a 20-layer grid 3D structure, applying photo-crosslinking every four layers (Fig. 8A). Each layer of this structure measured approximately 94.5 μm in height, closely matching the intended design of 100 μm.
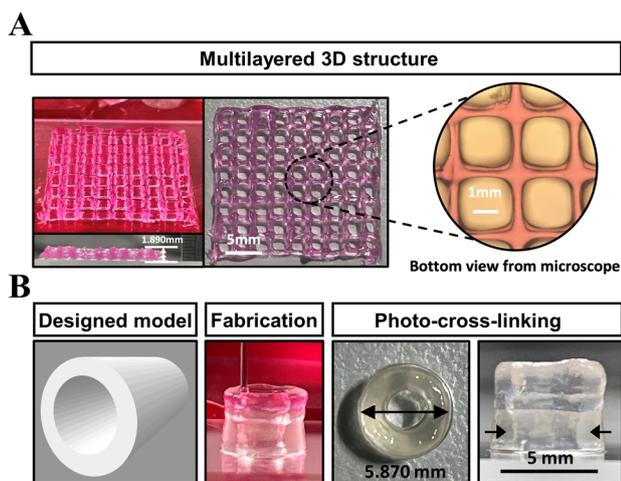
Fig. 8 Fabrication of multilayered 3D structures using ColME. (A) A grid pattern consisting of 1.8% ColME was bioprinted into a multilayered structure, applying photo-crosslinking every four layers. (B) A tubular structure, composed of 1.5% ColME, was bioprinted and subjected to a two-stage photo-crosslinking process.

Microscopic examination of the stacked layers demonstrated acceptable shape fidelity without any observable collapse from the bottom view. Periodic photo-crosslinking proved effective for constructing stable ColME 3D multilayered structures.

We also developed a tubular structure with outer and inner diameters of 6.0 mm and 2.5 mm, respectively, and a height of 5.0 mm (Fig. 8B). Each layer was printed in three concentric cycles. Upon reaching a height of approximately 3.1 mm, deformation occurred in the lower layers under the weight of the structure above (indicated by the black arrow). Photo-crosslinking was then applied to continue the stacking process. The structure eventually reached a height of 4.8 mm, after another round of photo-crosslinking, suggesting that ColME 3D structures require photo-crosslinking at approximately 3.0 mm in height to maintain structural integrity.

Compared to GelMA, ColME exhibits superior properties as a bioink for constructing 3D structures. GelMA is highly fluid at room temperature, requiring specialized techniques for stable multilayered construction. For instance, a freezing bed is often used as a platform to deposit GelMA structures to prevent collapse.[42,43] Another approach utilized a supporting bath to provide mechanical support during bioprinting before crosslinking, though this method is constrained by the scale of the structure.[44] In contrast, ColME is adaptable to ambient temperature printing environments without these constraints.

Cell viability in extruded ColME filaments

It is crucial for encapsulated cells within bioink to survive the bioprinting process. During bioprinting, cell death or adverse responses can occur due to extreme shear rates or stresses that may disrupt cell membranes.[5,22,45] To this end, cells were embedded in ColME solutions and extruded through 20G or 25G nozzles. We observed that cell encapsulation in ColME

solution increased the minimum extrusion pressure, ranging from 2.5 psi for 1.2% ColME to 5.5 psi for 2.0% ColME (S9 of the ESI†), indicating that cells act as particles that increase resistance to stress.

In the cell viability study, the cell-laden ColME solutions were extruded at various pressures based on ColME concentration and nozzle size. Live/dead staining of cell-laden ColME filaments showed that most cells survived in the filaments of 1.2%, 1.5%, and 1.8% ColME, while the majority of cells in 2.0% ColME died regardless of whether they were extruded through a 20G or 25G nozzle (Fig. 9A). Increasing the extrusion pressure by 1 psi through a 25G nozzle slightly increased cell death. Notably, dead cells were predominantly located near the surfaces of the filaments on the first day, likely due to higher shear near the nozzle wall. The proportion of live cells increased after 2 days of culture.

Quantitative analysis on day 0 showed that 84.8%, 90.1%, 78.0%, and 20.1% of cells were viable through a 25G nozzle for ColME concentrations of 1.2%, 1.5%, 1.8%, and 2.0%, respectively (Fig. 9B). Increasing the extrusion pressure by 1 psi through a 25G nozzle reduced viability to 78.7%, 87.1%, 70.4%, and 18.1%, respectively. Optimal cell viability was observed at 1.5% w/v ColME, with viability decreasing at higher concentrations. Cell survival through a 20G nozzle was higher compared to a 25G nozzle, particularly noticeable with 2.0% ColME (Fig. 9C). After two days of culture, cell viability significantly improved, particularly for 2.0% ColME, where viability increased to approximately 80% (Fig. 9D). Similarly, the viability of cells extruded through a 20G nozzle improved to over 80% regardless of ColME concentrations (Fig. 9E).

Our results indicate that cell viability immediately post-extrusion is acceptable with ColME concentrations from 1.2% to 1.8%, but not 2.0%. However, cells subsequently exhibit good growth within the ColME hydrogels.

We demonstrated that the high substitution of maleic groups in collagen confers several advantages. The alteration of pI makes ColME soluble in neutral environments, which is crucial for bioinks that require cell encapsulation. Additionally, increased maleate content enhances the crosslinking of collagen hydrogels, thereby improving both their mechanical properties and resistance to degradation. In many previous studies, the facilitation of collagen solution crosslinking required the addition of other synthetic or natural polymers for bioprinting. Common methods when printing collagen-based solutions were the combination of other natural or synthetic polymers to facilitate cross-linking, like alginate and fibrin.[46,47] The combination of alginate reinforced the cross-linking extent by ions and the simultaneous neutralization of collagen for gelation. Similar two-system cross-linking was also found by the addition of thrombin into fibrin and collagen neutralization. However, these methods complicate the printing process and prolong crosslinking times.[48] On the other hand, collagen with low methacrylate substitution is insufficient to form stable structures, necessitating the addition of extra methacrylated molecules to improve crosslinking.[21] Therefore, the development of highly
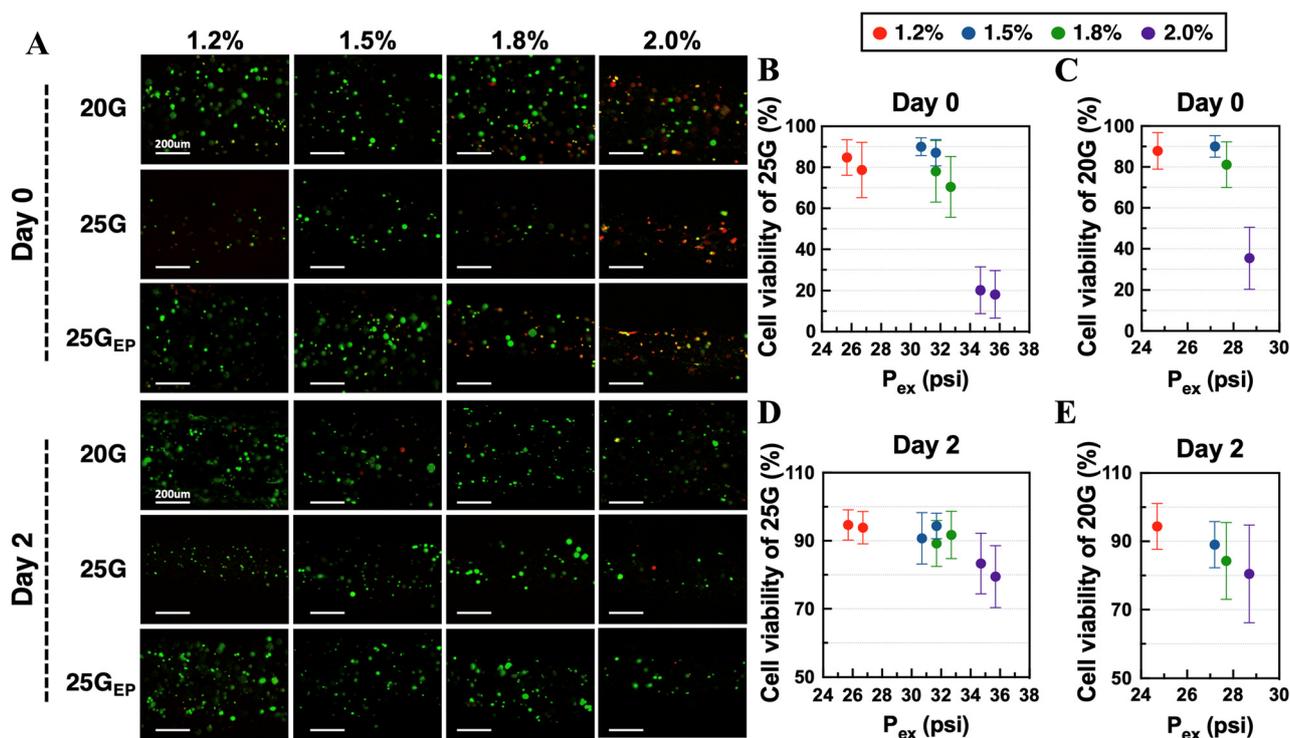
Fig. 9 Bioprinting of L929 encapsulated in various concentrations of ColME solution. (A) Assessment of cell viability using *Live/Dead* imaging for 20G, 25G, and 25G$_{EP}$ 1 psi more than 25G, with corresponding extrusion pressure (P_{ex}). The quantitated cell viability with (B) 25G and (C) 20G after extrusion, and after two days of culture with (D) 25G and (E) 20G. Sample number = 8, and error bars = standard deviation.

modified collagen was capable of providing mechanical support alone in a short period. Compared to GelMA, ColME, as a highly modified collagen, demonstrates greater resistance to enzymatic digestion, improved mechanical strength, and consistent printability regardless of temperature. These properties significantly mitigate the constraints associated with bioprinting using GelMA. In conclusion, ColME presents considerable advantages as a bioink component.

Conclusions

This comprehensive study has successfully demonstrated the potential of collagen maleate (ColME) as an innovative and effective bioink for 3D bioprinting applications. By chemically modifying bovine type I collagen with maleic anhydride to create a highly substituted ColME, we have achieved a bioink that is not only compatible with physiological pH but also retains the critical structural integrity of native collagen. Our findings highlight that the modification does not adversely affect the collagen's triple-helix structure, thereby maintaining its native properties which are essential for biological functions.

The optimization of bioprinting parameters, including ColME concentration, extrusion pressure, nozzle speed, and temperature, has facilitated the production of high-quality 3D structures. The use of intermittent photo-crosslinking has proven particularly effective in enhancing the structural integrity of multilayered constructs, which are stable enough for

complex tissue fabrication. Moreover, the mechanical and rheological evaluations confirm that ColME surpasses conventional bioinks such as methacrylated gelatin in terms of mechanical strength, enzymatic resistance, and overall printability.

Significantly, the cell viability studies embedded within this research illustrate that cells encapsulated within the ColME matrix exhibit high viability post-printing, indicating that the bioink supports not only the structural but also the biological aspects of tissue engineering. This dual functionality underscores the promise of ColME in regenerative medicine applications, where creating biologically active and mechanically robust tissues is crucial.

In conclusion, the synthesized ColME bioink presents a significant advancement in the field of 3D bioprinting. It holds considerable promise for future developments in tissue engineering and regenerative medicine, offering an excellent balance between biocompatibility, mechanical robustness, and functional performance. Further research and development will explore its applications across a broader range of tissues and investigate the long-term biological outcomes of its use in medical applications.

Author contributions

P.-H. Chen, investigation, formal analysis, design of methodology, writing—original draft; I.-H. Chen, investigation, formal

analysis, design of methodology; W.-H. Gao, investigation; S.-Y.W., investigation; W.-B.T., conceptualization, design of methodology, supervision, funding acquisition, writing— review and editing. All authors have read and agreed to the published version of the manuscript.

Data availability

Data is contained within the article.

Conflicts of interest

There are no conflicts to declare.

Acknowledgements

References

1 P. Bajaj, R. M. Schweller, A. Khademhosseini, J. L. West and R. Bashir, *Annu. Rev. Biomed. Eng.*, 2014, **16**, 247–276.

2 Y. S. Zhang, K. Yue, J. Aleman, K. Mollazadeh-Moghaddam, S. M. Bakht, J. Z. Yang, W. T. Jia, V. Dell'Erba, P. Assawes, S. R. Shin, M. R. Dokmeci, R. Oklu and A. Khademhosseini, *Ann. Biomed. Eng.*, 2017, **45**, 148–163.

3 S. Derakhshanfar, R. Mbeleck, K. G. Xu, X. Y. Zhang, W. Zhong and M. Xing, *Bioact. Mater.*, 2018, **3**, 144–156.

4 S. V. Murphy and A. Atala, *Nat. Biotechnol.*, 2014, **32**, 773–785.

5 S. Boularaoui, G. Al Hussein, K. A. Khan, N. Christoforou and C. Stefanini, *Bioprinting*, 2020, **20**, e00093.

6 H. Ravanbakhsh, V. Karamzadeh, G. Bao, L. Mongeau, D. Juncker and Y. S. Zhang, *Adv. Mater.*, 2021, **33**, 2104730.

7 Z. Wang, R. Abdulla, B. Parker, R. Samanipour, S. Ghosh and K. Kim, *Biofabrication*, 2015, **7**, 045009.

8 I. Parodi, D. Di Lisa, L. Pastorino, S. Scaglione and M. M. Fato, *Gels*, 2023, **9**, 482.

9 R. F. Pereira and P. J. Bartolo, *J. Appl. Polym. Sci.*, 2015, **132**, 1–15.

10 W. L. Ng, J. M. Lee, M. Zhou, Y.-W. Chen, K.-X. A. Lee, W. Y. Yeong and Y.-F. Shen, *Biofabrication*, 2020, **12**, 022001.

11 B. S. Kwak, W. Choi, J.-W. Jeon, J.-I. Won, G. Y. Sung, B. Kim and J. H. Sung, *J. Ind. Eng. Chem.*, 2018, **66**, 254–261.

12 B. J. Klotz, D. Gawlitta, A. J. Rosenberg, J. Malda and F. P. Melchels, *Trends Biotechnol.*, 2016, **34**, 394–407.

13 M. Poldervaart, B. Goversen, M. de Ruijter, A. Abbadessa, F. Melchels and F. Öner, *PLoS One*, 2017, **12**, e0177628.

14 B. Velasco-Rodriguez, T. Diaz-Vidal, L. C. Rosales-Rivera, C. A. García-González, C. Alvarez-Lorenzo, A. Al-Modlej, V. Domínguez-Arca, G. Prieto, S. Barbosa, J. F. A. Soltero Martínez and P. Taboada, *Int. J. Mol. Sci.*, 2021, **22**, 6758.

15 Y. Liu, S. C. Ng, J. S. Yu and W. B. Tsai, *Colloids Surf., B*, 2019, **174**, 316–323.

16 G. Ying, N. Jiang, C. Yu and Y. S. Zhang, *Bio-Des. Manuf.*, 2018, **1**, 215–224.

17 W. T. Brinkman, K. Nagapudi, B. S. Thomas and E. L. Chaikof, *Biomacromolecules*, 2003, **4**, 890–895.

18 Z. Wu, J. Liu, J. Lin, L. Lu, J. Tian, L. Li and C. Zhou, *Biomacromolecules*, 2022, **23**, 240–252.

19 M. K. Maher, J. F. White, V. Glattauer, Z. Yue, T. C. Hughes, J. A. M. Ramshaw and G. G. Wallace, *Polymers*, 2022, **14**, 1775.

20 K. Yang, J. Sun, Z. Guo, J. Yang, D. Wei, Y. Tan, L. Guo, H. Luo, H. Fan and X. Zhang, *J. Mater. Chem. B*, 2018, **6**, 7543–7555.

21 A. Mazzocchi, M. Devarasetty, R. Huntwork, S. Soker and A. Skardal, *Biofabrication*, 2018, **11**, 015003.

22 F. Garcia-Villen, A. Guembe, M. R. José, T. Zúñiga, S. Ruiz-Alonso, L. Saenz-del-Burgo, M. I. Jesús, I. R. José and J. L. Pedraz, *Int. J. Bioprint.*, 2023, **9**, 712.

23 Y. Yang, Z. Wang, Y. Xu, J. Xia, Z. Xu, S. Zhu and M. Jin, *Gels*, 2022, **8**, 314.

24 R. Sripriya, R. Kumar, S. Balaji, M. S. Kumar and P. K. Sehgal, *React. Funct. Polym.*, 2011, **71**, 62–69.

25 Z. Xu, X. Guan, J. Liu, H. Fan and Y. Chen, *J. Appl. Polym. Sci.*, 2017, **134**, 45424.

26 C. Li, H. Tian, L. Duan, Z. Tian and G. Li, *Int. J. Biol. Macromol.*, 2013, **57**, 92–98.

27 D. Pamfil, M. T. Nistor, L. F. Zemljic, L. Verestiuc, M. Cazacu and C. Vasile, *Ind. Eng. Chem. Res.*, 2014, **53**, 3865–3879.

28 S. Potorac, M. Popa, L. Picton, V. Dulong, L. Verestiuc and D. L. Cerf, *Biopolymers*, 2014, **101**, 228–236.

29 T. Lai, J. Yu and W. Tsai, *J. Mater. Chem. B*, 2016, **4**, 2304–2313.

30 G. K. Reddy and C. S. Enwemeka, *Clin. Biochem.*, 1996, **29**, 225–229.

31 N. Diamantides, C. Dugopolski, E. Blahut, S. Kennedy and L. J. Bonassar, *Biofabrication*, 2019, **11**, 045016.

32 N. Paxton, W. Smolan, T. Böck, F. Melchels, J. Groll and T. Jungst, *Biofabrication*, 2017, **9**, 044107.

33 A. Schwab, R. Levato, M. D'Este, S. Piluso, D. Eglin and J. Malda, *Chem. Rev.*, 2020, **120**, 11028–11055.

34 L. Ouyang, R. Yao, Y. Zhao and W. Sun, *Biofabrication*, 2016, **8**, 035020.

35 C. Li, Z. Tian, W. Liu and G. Li, *Mater. Sci. Eng., C*, 2015, **55**, 327–334.

36 N. J. Greenfield, *Nat. Protoc.*, 2006, **1**, 2876.

37 H. Liang, S. J. Russell, D. J. Wood and G. Tronci, *J. Mater. Chem. B*, 2018, **6**, 3703–3715.

38 M. Zhu, Y. Wang, G. Ferracci, J. Zheng, N.-J. Cho and B. H. Lee, *Sci. Rep.*, 2019, **9**, 1–13.

39 H. Nagase, A. J. Barrett and J. F. Woessner, *Matrix, Suppl. n1*, 1992, **1**, 421–424.

40 S. R. Caliari and J. A. Burdick, *Nat. Methods*, 2016, **13**, 405–414.

41 Z. Fu, S. Naghieh, C. Xu, C. Wang, W. Sun and X. Chen, *Biofabrication*, 2021, **13**, 033001.

42 H. Ding, N. P. Illsley and R. C. Chang, *Sci. Rep.*, 2019, **9**, 18854.

43 L. Siebert, E. Luna-Cerón, L. E. García-Rivera, J. Oh, J. Jang, D. A. Rosas-Gómez, M. D. Pérez-Gómez, G. Maschkowitz, H. Fickenscher and D. Oceguera-Cuevas, *Adv. Funct. Mater.*, 2021, **31**, 2007555.

44 A. Bhattacharyya, G. Janarthanan, T. Kim, S. Taheri, J. Shin, J. Kim, H. C. Bae, H.-S. Han and I. Noh, *Biomater. Res.*, 2022, **26**, 54.

45 A. Blaeser, D. F. Duarte Campos, U. Puster, W. Richtering, M. M. Stevens and H. Fischer, *Adv. Healthcare Mater.*, 2016, **5**, 326–333.

46 A. Isaacson, S. Swioklo and C. J. Connon, *Exp. Eye Res.*, 2018, **173**, 188–193.

47 A. Skardal, D. Mack, E. Kapetanovic, A. Atala, J. D. Jackson, J. Yoo and S. Soker, *Stem Cells Transl. Med.*, 2012, **1**, 792–802.

48 J. M. Unagolla and A. C. Jayasuriya, *Appl. Mater. Today*, 2020, **18**, 100479.